ORIGINAL PAPER

Exploring the effects of climate change on the water balance of a continuously moving deep-seated landslide

T. Zieher[1,2] · G. Gallotti[3] · G. Rianna[4] · A. Reder[4] · J. Pfeiffer[1,2]

Abstract

Impacts of expected climate change on the water balance in mountain regions may affect the activity of hydro-meteorologically driven deep-seated landslides. In the present study, an extended empirical monthly water balance model is used for reproducing the current and future hydro-meteorological forcing of a continuously moving deep-seated earth slide in Vögelsberg, Tyrol (Austria). The model extension accounts for effects of land cover and soil properties and relies on time series of air temperature and precipitation as data input. Future projections of the water balance are computed until the end of the twenty-first century exploiting a bias-corrected subset of climate simulations under the RCP8.5 concentration scenario, providing a measure of uncertainty related to the long-term projections. Particular attention is paid to the agreement/disagreement of the projections based on the selected climate simulations. The results indicate that a relevant proxy for the landslide's varying velocity (subsurface runoff) is generally expected to decrease under future climate conditions. As a consequence, it appears likely that the Vögelsberg landslide may accelerate less frequently considering climate change projections. However, the variability within the considered climate simulations still prevents results in full agreement, even under the 'most severe' scenario RCP8.5.

Keywords Landslide activity · Deep-seated earth slide · Water balance model · Climate change · EURO-CORDEX · OPERANDUM

✉ T. Zieher
Thomas.Zieher@oeaw.ac.at

1 Institute for Interdisciplinary Mountain Research, Austrian Academy of Sciences, Innrain 25, 6020 Innsbruck, Austria

2 Department of Geography, University of Innsbruck, Innrain 52f, 6020 Innsbruck, Austria

3 Department of Physics and Astronomy "Augusto Righi" (DIFA), University of Bologna, viale Berti-Pichat 6/2, 40127 Bologna, Italy

4 Regional Model and Geo-Hydrological Impacts (REMHI) Division, Fondazione Centro Euro-Mediterraneo Sui Cambiamenti Climatici, Via Thomas Alva Edison, 81100 Caserta, Italy

1 Introduction

Projected effects of climate change are expected to have an impact on the magnitude and frequency of natural hazards, including landslides (Gariano and Guzzetti 2016; Mora et al. 2018; Hock et al. 2019). Particularly in mountain regions, long-term changes in air temperature and precipitation may affect the hydro-meteorological drivers and triggers of landslides (Stoffel and Huggel 2012). On the one hand, related effects have been investigated in several retrospective studies comparing records of past landslide activity with paleoclimatic proxies, highlighting the strong relationship between landslides and climate (e.g. Lateltin et al. 1997; Borgatti and Soldati 2010, Panek 2019). On the other hand, prospective studies investigate the impacts of anthropogenic global warming on landslide activity by projecting their main hydro-meteorological forcing and geomechanical responses into the future (Gariano and Guzzetti 2016). For this purpose, relations between records of landslide activity and their hydro-meteorological drivers are first established and subsequently analysed based on downscaled projections of climate variables from general circulation models (GCMs) and regional climate models (RCMs) (Coe and Godt 2012). For both, retrospective and prospective studies, it is crucial to distinguish between landslide types, as they involve different hydro-meteorological drivers and triggering mechanisms (Crozier 2010; Sidle and Bogaard 2016; Jakob 2022).

Several prospective studies have addressed the impacts of climate change on rapid landslide types, typically triggered by extreme rainfall events, including debris flows (e.g. Stoffel et al. 2014; Turkington et al. 2016) and shallow landslides (e.g. Ciabatta et al. 2016; Rianna et al. 2017; Alvioli et al. 2018; Jakob and Owen 2021). However, the activity of continuously moving deep-seated landslides in soil is typically controlled by a slope's water balance and respective variations of pore water pressure which in turn govern the material's shear strength (Terzaghi 1950; Prokešová et al. 2013; Lacroix et al. 2020). Their reaction (acceleration and deceleration, typically with considerable temporal delay) depends on the respective type of movement and material, as well as local catchment characteristics, including topography (elevation range, hypsometry, aspect and slope), the geological setting (structural and stratigraphic properties), land cover, local climate peculiarities and human-induced drivers (Crozier 2010, Coe 2012, Jaboyedoff et al. 2016, Pfeiffer et al. 2021). With this respect, previous studies investigated the response of continuously moving deep-seated landslides to projected impacts of climate change on a case-study level. Buma and Dehn (1998) conducted one of the first studies combining climate projections with hydro-meteorological and slope stability models. Based on downscaled precipitation scenarios derived from the coupled GCM ECHAM4/OPYC3 (Roeckner et al. 1999), they used a conceptual hydro-meteorological model for computing recurrence intervals of identified groundwater thresholds and related landslide movement. In a related study, Dehn et al. (2000) investigated the future behaviour of a large mudslide in the Dolomites (northern Italy) by coupling the Thornthwaite water balance model (Thornthwaite and Mather 1955) with a limit equilibrium and a visco-plastic rheological approach. They calibrated the model with a displacement time series covering three years and computed projections of displacement until the end of the twenty-first century. Despite discussed limitations and uncertainties of the modelling chain, the results indicate that the displacement reduces under future climate conditions, with seasonal variations. Malet et al. (2005) employed the spatially distributed hydro-meteorological model STARWARS (Van Beek 2002) to investigate the dynamics of an earthflow in the Barcelonette catchment (south-eastern

French Alps). The authors parameterised the model based on extensive field and laboratory tests and calibrated it to reproduce observed groundwater levels. Using the downscaled climate projections from Buma and Dehn (1998), they computed projections of the groundwater level until 2060, indicating a decreasing average groundwater level and therefore a reduced activity of the landslide. Coe (2012) analysed a 12 yr time series of annual displacement measurements and correlated the long-term trend with a moisture balance drought index (MBDI), representing the hydro-meteorological forcing (groundwater pore pressure) of an earthflow in Colorado (United States). The author then computed MBDI time series using the mean of 36 downscaled climate projections based on the Intergovernmental Panel on Climate Change (IPCC) emission scenario A2 (Nakićenović et al. 2000), indicating a significantly reduced moisture balance and accordingly reduced landslide movement in future. Comegna et al. (2013) investigated the future behaviour of an earthflow in southern Italy by combining climate projections and a numerical model linking meteorological input to pore pressure response and the respective landslide movement. The authors calibrated the model based on available displacement time series covering three years. Using the calibrated model, Comegna et al. (2013) computed projections of displacement until 2060 based on air temperature and precipitation projections considering the IPCC A1B scenario (Nakićenović et al. 2000). The authors concluded that in the water balance, evaporation would increase and infiltration decrease due to the projected positive trend of mean air temperature and the reduction of precipitation. This would cause a gradual decrease in the groundwater level and, thus, a reduction of annual displacement.

The summarised previous studies investigate projected impacts of climate change on slowly moving deep-seated landslides in soil, employing different modelling techniques depending on the characteristics of the respective landslides and the available data. What they generally have in common is the conclusion that the activity of this type of landslide may decrease under future climate conditions. However, these studies are based on a single or a mean of multiple downscaled climate projections of respectively selected climate simulation chains (combined GCMs/RCMs), preventing conclusions about the agreement of the results based on different climate simulation chains. The present study explores impacts of climate change on the water balance and the related activity of a deep-seated landslide, individually considering five simulation chains under the Representative Concentration Pathway 8.5 (RCP8.5; Riahi et al. 2011). The individual results are analysed and compared, showing their agreement and disagreement in regard to future projections of the landslide's water balance. The study is embedded in the H2020 project OPERANDUM (Open-air laboratories for nature-based solutions to manage hydro-meteorological risks), aiming at identifying, implementing and evaluating nature-based solutions (NBS) against the impacts of various hydro-meteorological risks under current and future climate conditions (OPERANDUM 2022). These NBS are co-created together with scientific partners, local experts and stakeholders in the project's ten open-air laboratories (OALs), implemented for promoting innovation and research in a real-world setting. In the Austrian OAL, a continuously moving deep-seated landslide is investigated causing severe damage to buildings and infrastructure. Observed repeated acceleration phases are hydro-meteorologically controlled (Pfeiffer et al. 2021, 2022). It is therefore vital to investigate the impacts of climate change on the slope's water balance and related reactions of the landslide. Furthermore, modifications of the slope's water balance have been identified as potential NBS for reducing the landslide's activity, including an optimized forest cover (e.g. in terms of tree species composition) enhancing evapotranspiration in the hydrological catchment area. With this respect, the main objectives of the present study are to:

- Present and evaluate an extended version of the Thornthwaite model (Thornthwaite and Mather 1955; McCabe and Markstrom 2007), including effects of land cover on the water balance
- Establish projections of a landslide's water balance with the extended model, based on bias-corrected RCM simulations under RCP8.5
- Analyse the impacts of climate change on the future water balance and the landslide's response
- Draw conclusions about the agreement/disagreement between results based on the selected GCMs/RCMs
- Investigate the effects of a different forest type considered as NBS on the slope's water balance under current and future climate conditions

The extended water balance model is driven by bias-corrected simulations of five selected GCMs/RCMs of the EURO-CORDEX initiative (Jacob et al. 2014), representing a broad spectrum of future climate conditions under RCP8.5 and the uncertainty related to the long-term projections. In the following, the paper presents the investigated Vögelsberg landslide (Tyrol, Austria; Sect. 2) and the extended model, its sensitivity analysis and parameterisation, as well as the bias-correction procedure (Sect. 3). Section 4 presents the insights of the sensitivity analysis, resulting water balance components and their long-term trends and future changes relevant to the landslide's activity. The results are discussed in Sect. 5 before presenting the obtained conclusions in Sect. 6.

2 Study area–the Vögelsberg landslide

The Vögelsberg landslide is an earth slide located in the Eastern Alps about 20 km East of Innsbruck, Austria (Fig. 1a). The landslide is an active slab of a large deep-seated gravitational slope deformation (DSGSD) covering the entire slope with a planimetric area of about 5.5 km^2 ranging from approximately 800 to 2160 m a.s.l. The currently active part of the DSGSD covers an area of about 0.25 km^2, with its sliding surface reaching down to −48 m below the surface and is located in the lower section of the slope (Fig. 1b, c). Monitoring time series from an automatic total station revealed temporal dynamics of its velocity with acceleration phases attributed to varying hydro-meteorological input from prolonged moist periods and snow melt under current climate conditions (Pfeiffer et al. 2021). The geological setting is characterised by rocks belonging to the Innsbrucker Quartzphyllite complex (Rockenschaub et al. 2003). Different varieties of quartz phyllites occur in the study area, where differentiations regarding sericite-, chlorite- and calcite-content are obvious. Phyllite outcrops are abundant features, particularly in the upper catchment area. However, the soils have mainly developed from till, which has been dislocated by the DSGSD. At 11 locations, soil pits were excavated to investigate the soil type and depth. Cambisols dominate the catchment area, with patches of stagnic Cambisol and Gleysol (IUSS Working Group WRB 2014). Their depth ranges between 40 and 200 cm, with a mean value of 100 cm. At elevations above 1200 m a.s.l., the slope is mainly covered by spruce forests (*Picea abies* (L.) H. Karst) intertwined with larch (*Larix decidua* Mill.) and stone pine (*Pinus cembra* L.) stands in the uppermost part. Below 1200 m a.s.l., agricultural areas used as meadows and for pasture dominate with single forest patches in between (Fig. 1b). Residential and agricultural buildings are spread across the slope, and a group of houses is located
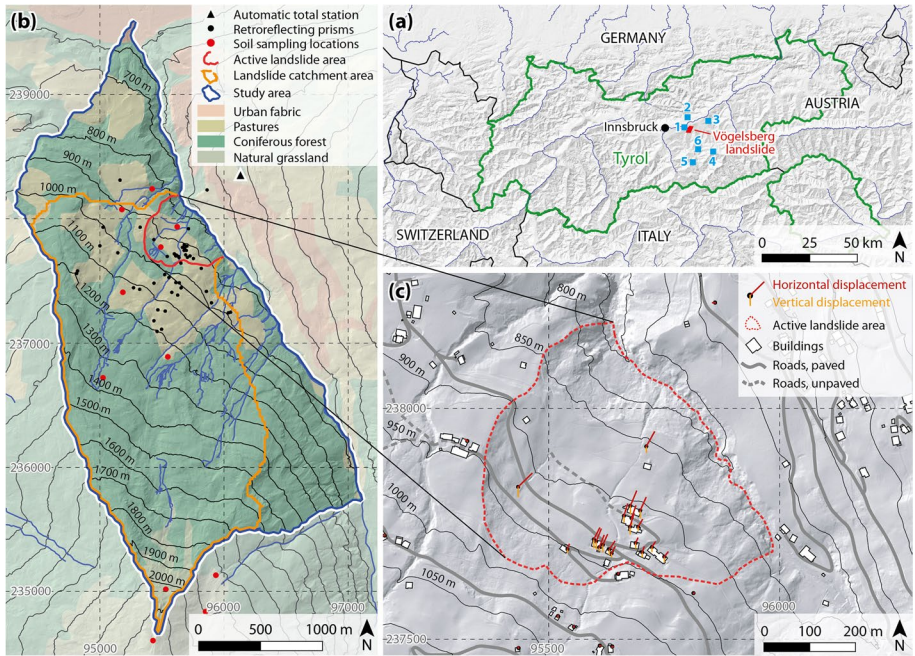
Fig. 1 Location of the Vögelsberg landslide and the considered meteorological stations (blue squares, numbering see Table S1) (**a**), overview of the study area and the catchment area of the Vögelsberg landslide with the latest Corine land cover (**b**) and map of the active landslide area with displacement vectors in horizontal (red) and vertical (orange) direction derived from the ATTS monitoring (**c**). The displacement vectors shown in (**c**) are exaggerated by a factor of 1000. Data source: Corine land cover 2018 (EEA 2018), airborne laser scanning and total station data: federal state of Tyrol, division of geoinformation. The data in (**b**) and (**c**) are shown in the Austrian GK West projection (EPSG 31254)

on top of the active landslide area, including respective infrastructure. Cracks in roads and buildings are abundant and visible indications of the landslide's activity. The landslide was continuously monitored with the help of an automated tracking total station (ATTS).

In a recent study, Pfeiffer et al. (2021) used a spatially distributed hydro-climatological model to investigate the hydro-meteorological drivers of the Vögelsberg landslide under present day conditions. Based on spatio-temporal analyses of snow melt, rainfall and evapotranspiration, the authors show that the acceleration phases generally correlate with snow melt in late winter and spring and with prolonged rainfall events. Enhanced ground water recharge and subsurface runoff, which lead to rising pore pressures during such moist periods, are the main drivers for the acceleration phases within the active landslide area. Furthermore, Pfeiffer et al. (2022) investigated the origin of the water responsible for the landslide's activity. The authors analysed the isotopic composition (stable oxygen and hydrogen isotopes) of water sampled at springs and from groundwater wells on the landslide body to infer its recharge areas using a novel geostatistical technique. They conclude that the main recharge areas are located along the ridge above the landslide, up to the uppermost area in the catchment above 2000 m a.s.l. Investigating projected changes of the water balance due to climate change and respective impacts on the landslide's activity must therefore consider the whole catchment area ranging up to 2160 m a.s.l.

3 Materials and methods

3.1 Extended monthly water balance model, sensitivity analysis and parameterisation

In the present study, the Thornthwaite water balance model (Thornthwaite and Mather 1955; McCabe and Markstrom 2007) has been adopted to compute the water balance of the landslide slope from observed and projected atmospheric variables (i.e. precipitation and air temperature). The model has been repeatedly modified and extended to include further physical processes (e.g. Graves and Chang 2007). In this work, relationships between land cover and physical processes have been added, including:

(1) For assessing evaporation, a crop coefficient K_c in line with the approach proposed by Allen et al. (1998): this modification permits to tailor evapotranspiration flows for different types of land cover assuming PET_{Hamon} (Hamon 1961) as a reference evapotranspiration ET_0;

(2) a variable runoff coefficient based on the Soil Conservation Service curve number (SCS-CN) approach (USDA 1986) aimed at including a runoff factor depending on monthly precipitation and different types of land cover following Ferguson (1996). The original SCS-CN is instead based on daily precipitation.

The extended model accounts for the major physical processes in the study area, including the differentiation of rain and snow, snow storage and snowmelt, infiltration, direct runoff, soil moisture storage, potential and actual evapotranspiration, and subsurface runoff (Fig. 2). The latter proved to be a suitable proxy for the activity of the Vögelsberg landslide.
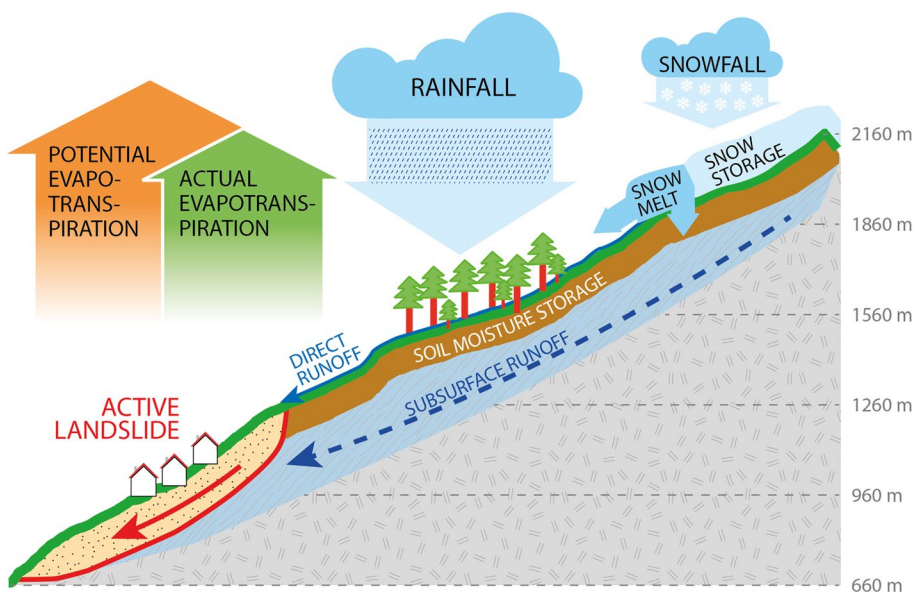

Fig. 2 Components of the conceptual monthly water balance model applied to the Vögelsberg landslide

During prolonged rainfall and snow melt periods, enhanced subsurface runoff leads to elevated groundwater levels, causing the landslide to accelerate (Pfeiffer et al. 2021).

Table 1 provides an overview of the equations adopted to model each physical process and the adopted parameter values. The modified Thornthwaite model was parameterised in three steps. First, the rain- and snowfall temperature thresholds and the maximum melt ratio were systematically tested. The individual model results were evaluated against observed snow cover time series at Kleinvolderberg station, located about 4 km West of the landslide area (station no. 1 in Fig. 1a). The best results were obtained using a snow-to-rainfall threshold of 2.0 °C, a precipitation-to-snowfall threshold of −0.2 °C and a maximum melt ratio of 0.8. Generally, the adopted values agree with the range reported in scientific literature although they vary considerably depending on respective site-specific conditions (Bock et al. 2016; Hay and McCabe 2010; Jennings et al. 2018; You et al. 2014).

In a second step, a one-at-a-time (OAT) sensitivity analysis (e.g. Zieher et al. 2017) was performed to assess the impact of the introduced crop coefficient, the parameters related to the SCS curve number and the volumetric water content at field capacity. Respective value ranges and central values were adopted from scientific literature (Table 2). The central value of the soil water content at field capacity of 34.7% was derived from respective recordings at the 11 excavated soil profiles. Also the soil depth was retrieved from the soil profiles, ranging from 0.4 to 2.0 m and a mean value of 1.0 m.

In a third step, the computed subsurface runoff was evaluated against landslide velocity time series in order to identify a set of parameter values representing the current hydro-meteorological forcing of the landslide. Landslide velocity was derived from an ATTS installed in May 2016 on the opposite side of the valley (Fig. 1b). The ATTS monitoring included 53 retroreflecting prisms distributed across the active landslide area (n = 20) and the comparably stable surrounding (n = 33). The monthly mean velocity covering May 2016 to October 2019 was correlated with the subsurface runoff computed with the model, considering various settings of the identified sensitive parameters (crop coefficient and SCS curve number). To account for the delayed response of the landslide (Pfeiffer et al. 2021), running sums over different periods were considered. The resulting best-performing set of parameter values was then adopted for applying the model with the climate projections.

3.2 Climate model data and bias correction

Five climate modelling chains among those made available by the EURO-CORDEX initiative (Jacob et al. 2014) were selected (Table 3) to assess the potential changes of the landslide's hydro-meteorological forcing due to climate change. The CORDEX initiative is an international framework for the voluntary cooperation of international partners, aiming at improving climate change projections at regional scale with world-wide coverage (Giorgi et al. 2009). The European branch EURO-CORDEX provides dynamical and statistical downscaling for a fixed domain over Europe at different horizontal resolutions (the finest one equal to about 12 km (0.11°). For what concerns dynamical downscaling, the EURO-CORDEX ensemble exploits GCMs provided by the Coupled Model Intercomparison Project (CMIP, Meehl et al. 2000) over which RCMs are nested, while adopting a consistent spatial domain and gridding to enhance the combinability and comparability of the simulations. However, due to time and resource constraints required to run climate simulations, the EURO-CORDEX initiative may lag behind the latest advancements of GCMs (e.g. migration from CMIP phase 5 to CMIP phase 6 models). Furthermore, ensemble simulations are usually run at a horizontal resolution accounting for several constraints,

Table 1 Equations adopted for each modelled physical process with parameters defined for the present case study

Physical process	Formulation	Variables
(1) Rain and snow	$P_{snow} = P$ when $T \leq STT$ $P_{snow} = 0$ when $T \geq RTT$ $P_{snow} = P \times [(RTT - T)/(RTT - STT)]$ otherwise $P_{rain} = P - P_{snow}$	T (°C) = monthly air temperature P (mm) = monthly total precipitation P_{rain} (mm) = monthly rainfall P_{snow} (mm) = monthly snowfall RTT (°C) = rainfall temperature threshold = 2.0 °C STT (°C) = snowfall temperature threshold = −0.2 °C
(2) Snow cover and snow melt	$SSTOR = SD_{i-1} + P_{snow}$ $SM = SSTOR \times [(T - STT)/(RTT - STT)] \times MMAX$ $SD_i = SSTOR - SM$	i = current month $SSTOR$ (mm) = accumulated snow storage SD (mm) = monthly snow depth as equivalent water SM (mm) = amount of snow melted in a month $MMAX$ = maximum melt rate = 0.80
(3) Direct runoff	$DR = 25.4 \times [a + b \times (P_{rain}/25.4) / (S \times k)]$ $S = (1000/CN) - 10$	DR (mm) = monthly surface runoff a, b, k = empirical parameters obtained by interpreting precipitation observed at the Kleinvolderberg station for different CN values (Ferguson 1996); a = −1.024; b = 0.500; k = 0.374 CN (soil curve number) = 55
(4) Infiltration	$I = P_{rain} - DR + SM$	I (mm) = monthly infiltration
(5) Potential evapotranspiration	$PET_{Hamon} = 13.97 \times d \times D2 \times W_t$ $W_t = [4.95 \times \exp(0.062 \times T)]/100$ $PET = kc \times PET_{Hamon}$	PET_{Hamon} (mm) = monthly potential evapotranspiration based on (Hamon 1961) PET (mm) = monthly potential evapotranspiration (derived for a specific land cover) kc (crop coefficient) = 1.20 d = number of days in a month D = mean monthly hours of daylight in units of 12 h W_t (g/m³) = saturated water vapour density term
(6) Actual evapotranspiration	$AET = PET$ when $I > PET$ $AET = abs(I - PET) \times (SM_i - 1/SMFC) + I$ otherwise $SMFC = z \times fc$	AET (mm) = monthly actual evapotranspiration SM (mm) = soil moisture, $SMFC$ (mm) = soil moisture at field capacity z (mm) = soil depth = 1000 mm fc = volumetric water content at field capacity = 0.347
(7) Soil moisture	$SM_i = SM_i - 1 + I - AET$ surplus = 0 when $SM_i < SMFC$ surplus = $SM_i - SMFC$ && $SM_i = SMFC$ otherwise	surplus (mm) = water exceeding field capacity and available for sub-surface runoff

Table 1 (continued)

Physical process	Formulation	Variables
(8) Subsurface runoff	$\text{tot\_surplus}_i = (\text{tot\_surplus}_{i-1} + \text{surplus}) \times (1 - \text{srf})$ $SR = (\text{tot\_surplus}_{i-1} + \text{surplus}) \times \text{srf}$	tot_surplus (mm) = total surplus available for next month srf = subsurface runoff factor = 0.50 SR (mm) = subsurface runoff
(9) Total runoff	$R = DR + SR$	R (mm) = total runoff

Table 2 Parameter value ranges and central values for the OAT sensitivity analysis

	Soil moisture capacity	Curve number	Crop coefficient
Minimum value	0.100	30	0.600
Central value	0.347	55	0.785
Maximum value	0.400	90	1.500

including (i) the computational resources of the involved voluntary institutions, (ii) the time spans of analyses to proper characterise interannual variability under several scenarios of greenhouse gas concentrations and (iii) the added value of high spatial resolutions for reproducing local weather patterns (Kendon et al. 2021; Pichelli et al. 2021). In the present study, the concurrently available EURO-CORDEX ensemble simulations based on GCMs of CMIP phase 5 are used, which are considered feasible for the investigation of climate change impacts (e.g. Feyen et al. 2020).

The selection of the five modelling chains has been carried out for all OALs investigated within the OPERANDUM project, exploiting multiple climate simulation chains, considering the same evolution of greenhouse gas concentrations as suggested by the Representative Concentration Pathway 8.5 (RCP8.5; Riahi et al. 2011). The RCPs are a common set of concentration pathways based on socio-economic scenarios, which are used as input for climate simulations by the scientific community. These pathways were developed in the framework of the IPCC's Fifth Assessment Report (IPCC 2014) for assessing climate impacts and deducing mitigation strategies (van Vuuren et al. 2011). The suffixes identify the expected increase in radiative forcing by 2100 compared to the pre-industrial era (i.e. 8.5 W/m^2 in case of RCP8.5). In this regard, RCP8.5 represents a fossil-fuel-intensive scenario excluding any mitigation policies, entailing the most severe impacts of climate change. Despite its reliability and actual usefulness for developing climate policies is widely debated in the literature (e.g. Hausfather and Peters 2020; Schwalm et al. 2020), it has been selected in the framework of the OPERANDUM project to consider the most severe impacts of climate change on the hydrological cycle in the context of different natural hazards. Furthermore, following Sanderson (2018), the project aims at providing a framework that is easily scalable and reproducible while providing insights about the uncertainties associated with the modelling.

In this regard, it is worth noting that EURO-CORDEX and their sub-selection represent an 'ensemble of opportunity' where all the uncertainty sources could not be adequately accounted for and quantified. Therefore, the full ensemble could also represent a lower boundary of uncertainties affecting the evaluation of future evolution in weather forcing. On the other hand, the subsample tries to identify a large range of equilibrium climate sensitivity (ECS) of GCMs, defined as the equilibrium change in annual global mean surface temperature following a doubling of the atmospheric concentration of carbon dioxide relative to pre-industrial levels. Specific sensitivity analyses for GCMs usually assess ECS; the numbers shown in Table 3 are based on Meehl et al. (2020) and Wyser et al. (2020).

Despite the increasing performance of RCMs, the limitations in orographic representations and in sub grid processes, for which physical parameterisations are required, could induce a limited representation of the atmospheric physics (in particular for short-duration precipitation related to the convective instability), preventing a direct use of atmospheric variables in impact models. To reduce this error assumed as systematic, the scientific community is developing numerous statistical procedures, acknowledged as bias correction

Table 3 Metadata of the selected EURO-CORDEX data. GCM: general circulation model, ECS: equilibrium climate sensitivity, RCM: regional climate model

No	Institution	GCM	ECS [°C]	RCM	Period
1	Irish centre for high end computing (ICHEC)	EC-EARTH	3.3	RACMO22E	1950/01/01–2100/12/31
2	Irish centre for high end computing (ICHEC)	EC-EARTH	3.3	CCLM4-8-17	1949/12/01–2100/12/31
3	Met office Hadley centre (MOHC)	HadGEM2-ES	4.6	SMHI-RCA4	1970/01/01–2099/12/30
4	Max–Planck-institute (MPI)	MPI-ESM-LR	3.6	SMHI-RCA4	1970/01/01–2100/12/31
5	Norwegian climate centre (NCC)	NorESM1-M	2.8	DMI-HIRHAM5	1951/01/01–2100/12/31

(BC) techniques, able to 'adjust' the raw model output towards observations in a post processing step (Maraun and Widmann 2018).

In this work, the scaled distribution mapping (SDM) procedure (Switanek et al. 2017) has been adopted to 'adjust' RCM outputs. This technique preserves the changes projected by the climate model in the bias-corrected series, avoiding assumptions about stationarity. Operatively, the SDM scales the observed distribution by raw model projected changes in magnitude, rain-day frequency (for precipitation), and the likelihood of events according to the bias correction period. In this perspective, the period from 1981 to 2010 has been used as a reference (REF) according to the World Meteorological Organization guidelines for current conditions (WMO 2017), while the time span up to 2100 has been adjusted.

For precipitation bias correction, the SDM procedure considers only values of positive precipitation exceeding a specified threshold (e.g. 0.1 mm) and a multiplicative or relative amount as a scaling factor. For temperature bias correction, the SDM procedure is applied, considering all temperature values and using an absolute amount as a scaling factor. Moreover, temperature data are first de-trended, then bias corrected, and finally, the trends are added again. This avoids that temporal trends inflate the variance.

3.3 Water balance projections and evaluation of effects of climate change and land use change

The parameterised model, reproducing the landslide's hydro-meteorological forcing, was then applied with the bias-corrected projections of air temperature and precipitation. To account for the vertical range of the landslide's effective hydrological catchment and because the water balance is strongly affected by the steep hydro-climatological gradients in mountain areas, projections of the water balance were computed for elevation steps from 660 to 2160 m a.s.l. with 300 m increments (Pfeiffer et al. 2021, 2022). Monthly gradients of air temperature and precipitation were computed from in situ observations of six meteorological stations in the vicinity of the study area (see Fig. 1a and Table S1 in the supplement material). Particularly air temperature shows a significant gradient and a seasonal variation, while precipitation does not show distinct gradients. To account for the temperature decrease with altitude, the median monthly gradients were adopted for preparing the temperature projections for the application of the model across the vertical elevation range.

For assessing changes in the projected water balance and the related activity of the Vögelsberg landslide, two indicators were analysed for each GCM/RCM and the considered elevation steps. They are both based on the subsurface runoff cumulated over three months (SR_{cum}) and include its seasonal maximum (SR_{max}) and the seasonal frequency of SR_{cum} exceeding a threshold of 100 mm. SR_{max} represents the general activity of the landslide in terms of velocity, with low and high subsurface runoff correlated with low and high landslide velocity, respectively. Long-term trends of projected SR_{max} are derived, indicating changes in landslide velocity under future climate conditions. The frequency of $SR_{cum} > 100$ mm corresponds to the frequency of landslide acceleration phases, during which differential movements are induced on the landslide body, causing major damage to the settlement and infrastructure travelling on top. Both indicators are evaluated seasonally to consider their annual cycles. Changes in the frequency of $SR_{cum} > 100$ mm were analysed relative to the REF period (1981–2010) for 30-year periods mid of the century from 2021 to 2050 (MID) and towards the end of the century from 2071 to 2100 (END).

In a next step, projections of the water balance were obtained for a land cover/land use scenario replacing the contemporary coniferous forest with a mixed forest in the upslope

catchment area of the landslide. This intervention is considered as a potential long-term NBS to reduce the landslide's activity. The areas covered by pasture remained unchanged in this scenario. The crop coefficient was raised to 1.3 and a curve number of 56 was used. The evaluation of both indicators was repeated, comparing the results for the REF, MID and END periods relative to the results with the original land cover parameterisation.

4 Results

4.1 Sensitivity analysis and parameterisation

The conducted OAT sensitivity analysis revealed that variations of the crop coefficient (kc) have the highest impact on the resulting median of subsurface runoff considering the reference period from 1981 to 2010 ($-$ 99 to $+$30%, Fig. 3a). Also the SCS curve number (SCS-CN) has a distinct impact on the resulting median of subsurface runoff ($-$ 34 to $+$4%, Fig. 3a). The soil water content at field capacity (fc) does not lead to substantial changes in subsurface runoff in the considered case study (0.0 to $+$0.3%, Fig. 3a). The results of the parameter tests combined with varying accumulation periods of the resulting subsurface runoff show that the running sum over three months provides the best agreement with the observed landslide velocity (Fig. 3b, c). The best result was obtained for a crop coefficient of 1.2 and the SCS curve number 55. These parameter values were used for applying the model with the climate projections across the considered elevation steps.

4.2 Landslide dynamics and current hydro-meteorological forcing represented by the model

The available time series derived from the ATTS monitoring show a continuous movement of the active landslide area of at least 1 cm/yr (Fig. 4a). The kinematic behaviour is characterised by acceleration and deceleration phases which are clearly not related to seasonal or other cyclically occurring causes. In the course of the three main acceleration phases, the velocity increases up to almost 6 cm/yr in August 2016, to around 5 cm/yr in November 2017, and about 3 cm/yr in March 2019. While the velocity decreases sharply after the peak in mid-2016, the movement rate decreases more gradually after the maximum at
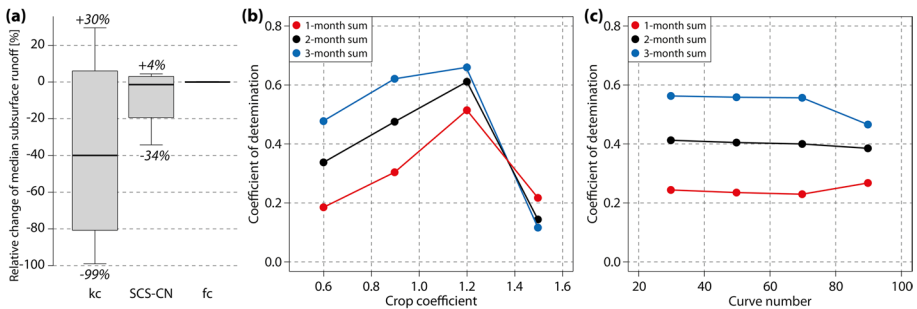

Fig. 3 Results of the OAT sensitivity analysis (**a**) and the parameter tests for the crop coefficient (**b**) and curve number (**c**) considering different accumulation periods for the resulting subsurface runoff. The model results were evaluated against the monthly median displacement time series by fitting linear models, considering their coefficient of determination as performance
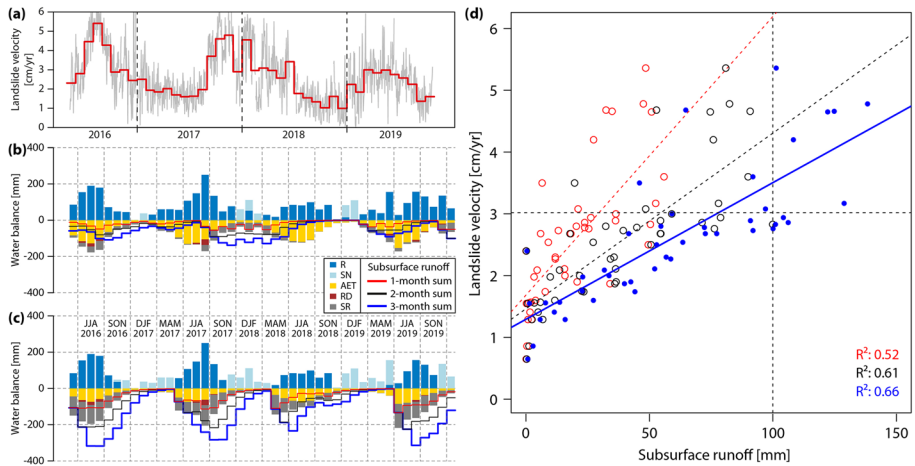
Fig. 4 Time series of landslide velocity derived from the ATTS monitoring on a daily resolution (**a**; grey) and aggregated to monthly medians (**a**; red) and monthly water balance components at 660 m a.s.l. (**b**) and 2160 m a.s.l. (**c**). Correlation between monthly landslide velocity and the derived subsurface runoff (**d**) per month (red) and cumulated over two (black) and three months (blue) between 2016/05 and 2019/10. R: rainfall, SN: snow, AET: actual evapotranspiration, RD: direct runoff, SR: subsurface runoff

the end of 2017 and spring 2019. Pfeiffer et al. (2021) show that the first two acceleration phases are related to prolonged moist conditions with above-average rainfall sums. In the acceleration phase in early 2019, infiltrating melt water from snow melt starting on the lower part of the slope is identified as the main hydro-meteorological driver. Furthermore, the landslide shows delayed reactions to the hydro-meteorological forcing of up to 60 days (Pfeiffer et al. 2021).

The resulting water balance components based on the identified parameterisation are shown for 660 m a.s.l. (Fig. 4b) and 2160 m a.s.l. (Fig. 4c), comparing incoming rainfall (R) and snow (SN) (positive) with outgoing components, including the actual evapotranspiration (AET), direct runoff (RD), and subsurface runoff (SR). Obvious differences concerning the amount of snow are mainly related to the lower temperatures with increasing altitude. In general, the winters in 2017/18 and 2018/19 have been exceptionally snow-rich in the Tyrolean Alps (Andre et al. 2019, ZAMG 2022). The reduced actual evapotranspiration resulting at 2160 m a.s.l. compared to 660 m a.s.l. can be again attributed to the lower temperature. The direct and subsurface runoff components are more pronounced at high elevation in the late spring and early summer season due to rapid snow melt and the higher availability of water in the soil due to lower atmospheric demand. At lower elevations, the outgoing components are more balanced over the year. Direct runoff mainly occurs during the summer months as a response to excessive rainfall.

The subsurface runoff (SR) component rises as a response to snow melt and during periods of enhanced rainfall. Particularly at low elevations, the resulting SR does not show distinct seasonal patterns and generally matches the acceleration and deceleration phases of the landslide. The subsurface runoff component of the water balance model cumulated over three months shows the best agreement with the monthly landslide velocity (Fig. 4d). The respective relationship shows that above a threshold of 100 mm per month the landslide moves at approximately 3 cm/year or faster. This threshold is subsequently used to assess

the occurrence of hydro-climatological conditions favouring the landslide's acceleration under future conditions.

4.3 Trends in the bias-corrected GCM/RCM projections

For the computation of future projections of the monthly water balance, the model was driven with five bias-corrected EURO-CORDEX projections of air temperature and precipitation. Figure 5 shows bias-corrected seasonal projections of mean air temperature and fitted trends from 1981 to 2100 and observations from 1981 to 2019 at Kleinvolderberg station (660 m a.s.l.). All observed trends of the projections indicate a statistically significant increase in mean air temperature. For the winter (DJF), spring (MAM) and summer season (JJA), the trends of mean seasonal air temperature projected by the GCMs/RCMs HadGEM2-ES/RACMO22E, EC-EARTH/CCLM4-8-17 and NorESM1-M/DMI-HIRHAM5 are in good agreement with observed trends. The GCMs/RCMs HadGEM2-ES/SMHI-RCA4 and MPI-ESM-LR/SMHI-RCA4 project a distinctly higher increase in mean seasonal air temperature compared to the other GCMs/RCMs and observed trends. In the fall season (SON), the trends vary with HadGEM2-ES/SMHI-RCA4 projecting the highest
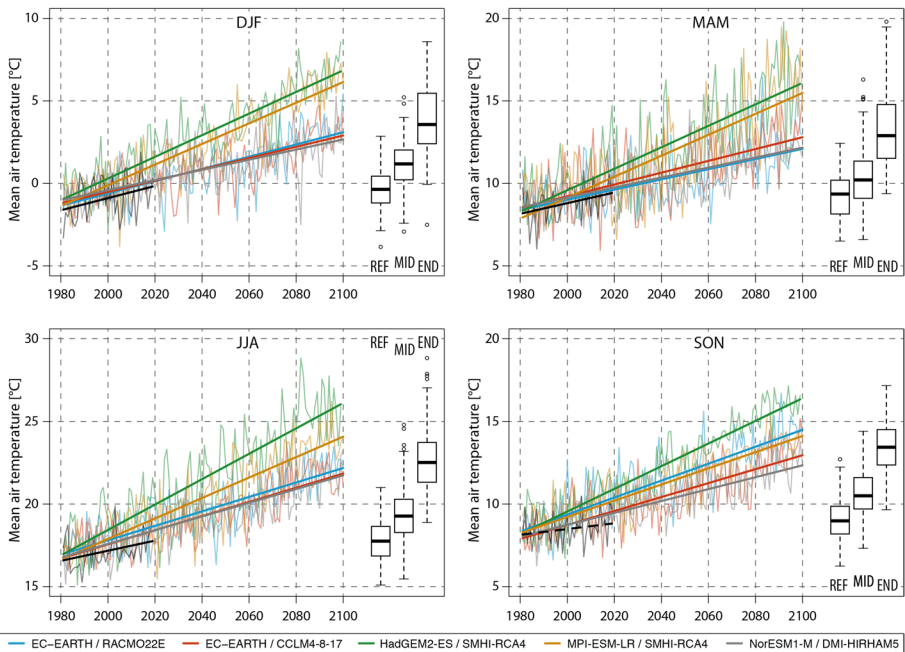

Fig. 5 Seasonal trends of mean air temperature from observations (1981–2019; black lines) and future projections from bias-corrected EURO-CORDEX data at the meteorological station Kleinvolderberg (660 m a.s.l.). The thin lines show the mean seasonal air temperature (aggregated per year) and the thick lines show the linear trends in the respective colours. The boxplots show the distribution of all GCMs/RCMs combined for the reference period REF (1981–2010), MID of the century (2021–2050) and END of the century (2071–2100). All shown linear trends are statistically significant at a significance level of 0.05 (solid lines), except for the observation data in the fall season (dashed black line). DJF: December–January–February; MAM: March–April–May; JJA: June–July–August; SON: September–October–November. The boxplots show the median, the 25 and 75% quantiles (box), the value range of 1.5 times the interquartile range (whiskers) and outliers beyond that

and NorESM1-M/DMI-HIRHAM5 showing the lowest temperature increase. The observed temperature trend shows an even lower gradient but is not statistically significant.

The bias-corrected precipitation projections do not reveal consistent seasonal trends with all considered GCMs/RCMs in agreement (Fig. 6). For the winter (DJF) and spring (MAM) seasons, three out of five GCMs/RCMs project a slight increase while the remaining two indicate no change. For the summer season (JJA), three out of five GCMs/RCMs project a distinct negative trend while the variance of the projected seasonal precipitation sums (aggregated per year) is markedly higher than for the other seasons. However, the subset of GCMs/RCMs pointing to similar changes in the winter, spring and summer seasons is not consistent. For the fall season (SON), only NorESM1-M/DMI-HIRHAM5 projects a distinct increase in precipitation while the other GCMs/RCMs do not reveal changes. None of the observed seasonal precipitation trends is statistically significant.

4.4 Projected changes in the seasonal maximum of subsurface runoff

As shown above, the subsurface runoff cumulated over three months correlates well with the time-varying landslide velocity for 2016–2019. In general, the absolute amount of
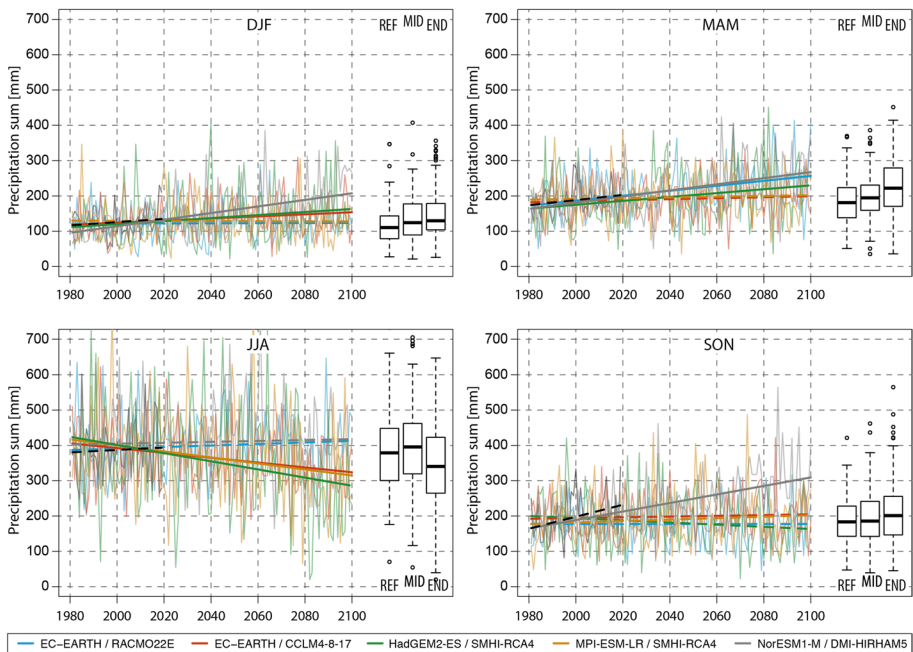

Fig. 6 Seasonal trends of precipitation sum from observations (1981–2019; black lines) and future projections from bias-corrected EURO-CORDEX data at the meteorological station Kleinvolderberg. The thin lines show the seasonal precipitation sums (aggregated per year) and the thick lines show the linear trends in the respective colours. The boxplots show the distribution of all GCMs/RCMs combined for the reference period REF (1981–2010), MID of the century (2021–2050) and END of the century (2071–2100). Statistically significant linear trends at a significance level of 0.05 are shown as solid lines. DJF: December–January–February; MAM: March–April–May; JJA: June–July–August; SON: September–October–November. The boxplots show the median, the 25 and 75% quantiles (box), the value range of 1.5 times the interquartile range (whiskers) and outliers beyond that

subsurface runoff increases with elevation (Fig. 7). Combining the results based on the considered GCMs/RCMs at 660 m, the mean annual maximum of 3 months-cumulated subsurface runoff amounts to 60 mm/yr (ca. 7% of the mean annual precipitation sum) in the REF period, whereas at 2160 m around 160 mm/yr (ca. 18% of the mean annual precipitation sum) are reached. This difference is owing to the reduced evapotranspiration resulting from the lower temperatures at high elevation. The seasonality of SR_{max} is more pronounced at high elevations, mainly due to the seasonality of precipitation, the predominantly solid precipitation during the winter and early spring season and the delayed snow melt compared to low elevations. The seasonal trends generally suggest a reduction of the SR_{max} under future climate conditions, except for the results based on NorESM1-M/DMI-HIRHAM5, which instead suggests an increase particularly in the winter and spring seasons and, at high elevation, also during the summer season.

Figure 8a shows the gradients of the linear models fitted to the projected SR_{max} (shown in Fig. 7) as a function of elevation, with the colour indicating the underlying
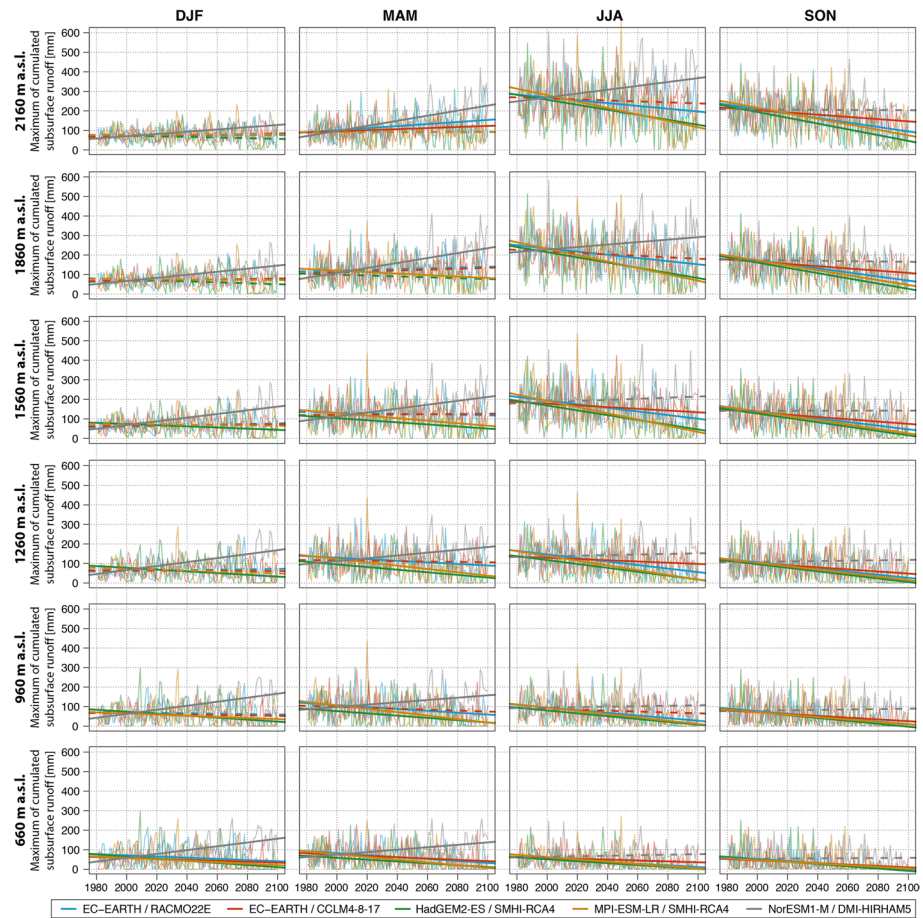

Fig. 7 Resulting projections of the seasonal maximum of subsurface runoff cumulated over three months (1981–2100) at the considered elevation steps. The linear trends shown as solid lines indicate statistically significant results, dashed lines fall below the 95% confidence
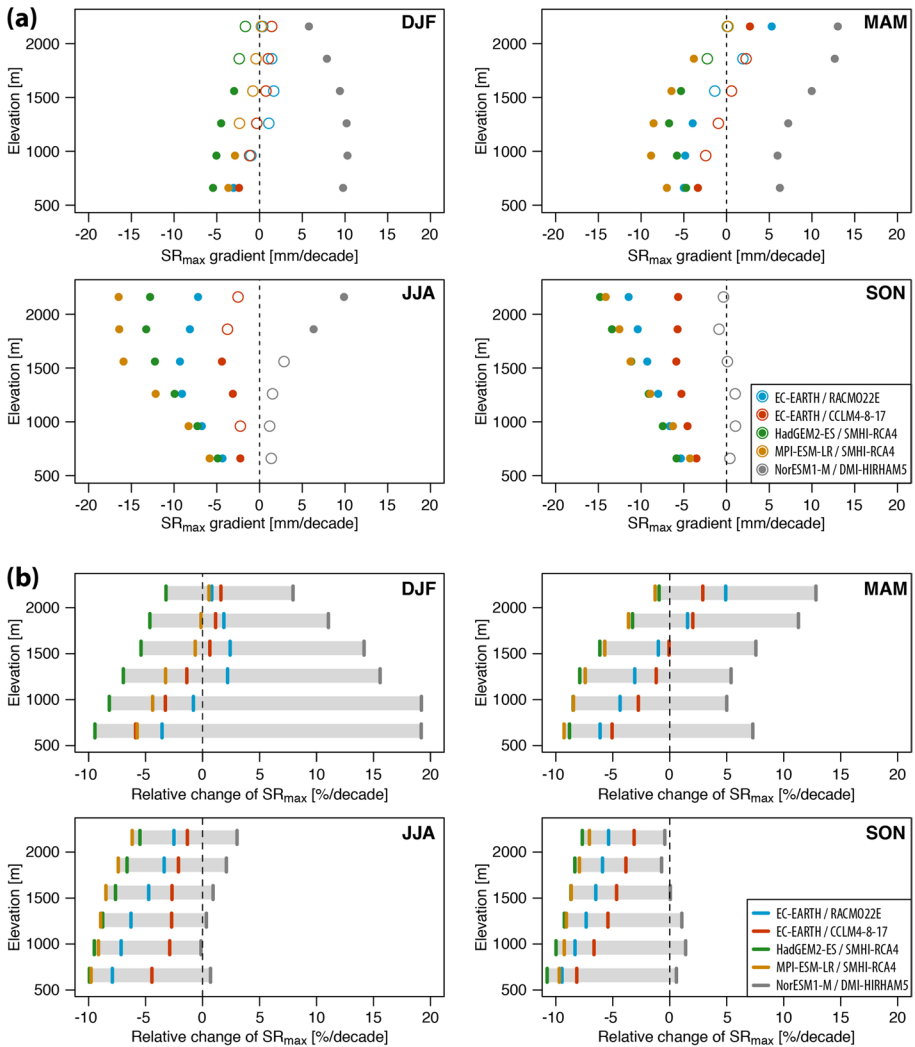
Fig. 8 Seasonal gradients of the long-term linear trends of SR_{max} (1981–2100; **a** and relative change of mean SR_{max} during the REF and END periods **b** per GCM/RCM at the considered elevation steps. Statistically significant trends (significance level of 0.05) in (**a**) are shown as dots. Positive gradients indicate an increase, negative gradients a decrease over the considered period

GCM/RCM. Positive values refer to an increase of SR_{max} during the considered period from 1981 to 2100, while negative values indicate a reduction. Trends suggesting significant changes are shown as filled dots, non-significant trends as circles. In general, the results based on the models EC-EARTH/RACMO22E, EC-EARTH/CCLM4-8-17, HadGEM2-ES/SMHI-RCA4 and MPI-ESM-LR/SMHI-RCA4 show similar, mostly negative trends of SR_{max} across the considered elevation steps. However, the results based on NorESM1-M/DMI-HIRHAM5 differ considerably, indicating mainly positive trends, particularly in the winter and spring seasons. In Fig. 8b, the relative seasonal changes of

mean SR_{max} during the REF and END periods are shown considering the GCMs/RCMs and elevation steps. The relative changes generally reflect the shown long-term trends (Fig. 8a) but emphasize the sensitivity of the projected absolute changes of SR_{max} per season.

For the winter season, the results based on the NorESM1-M/DMI-HIRHAM5 model indicate positive trends with an increase of SR_{max} up to 9.8 mm/decade in low and medium elevations up to 1500 m. This corresponds to a significant increase of $+19.2\%$/decade at 960 m, comparing the means of SR_{max} in DJF during the REF and END periods. The results based on the other considered models indicate minor negative trends only significant at low elevations with gradients between -2.4 and -5.4 mm/decade at 660 m, corresponding to -3.5 to -9.5%/decade comparing the means of SR_{max} in DJF during the REF and END periods. For the winter season, SR_{max} is therefore projected to either increase markedly (results based on one GCM/RCM) or decrease slightly at low elevations (results based on four GCMs/RCMs).

For the spring season, the resulting gradients based on NorESM1-M/DMI-HIRHAM5 are generally positive, with higher values of up to 13.0 mm/decade ($+12.8\%$/decade comparing the means of SR_{max} in MAM during the REF and END periods) in the uppermost elevation steps considered. The other results suggest a significant decrease in SR_{max} particularly in low and medium elevations. The results based on EC-EARTH/CCLM4-8-17 and MPI-ESM-LR/SMHI-RCA4 indicate a decrease in SR_{max} of -2.4 and -8.8 mm/decade at 960 m respectively, corresponding to -2.7 and -8.5%/decade comparing the means of SR_{max} in MAM during the REF and END periods. For the spring season, SR_{max} is projected to either increase particularly at high elevation (results based on one GCM/RCM) or decrease at low and mid elevation (results based on four GCMs/RCMs).

For the summer season, the results based on NorESM1-M/DMI-HIRHAM5 indicate significant positive trends in SR_{max} only in the uppermost elevation steps of up to 9.9 mm/decade ($+3.0\%$/decade comparing the means of SR_{max} in JJA during the REF and END periods). In contrast, the results based on the models HadGEM2-ES/SMHI-RCA4 and MPI-ESM-LR/SMHI-RCA4 show a distinct decrease in SR_{max}, which increases with elevation. The results obtained with the model EC-EARTH/RACMO22E show the same trends as the latter for the lower elevation steps but less pronounced negative trends at high elevations. Results based on EC-EARTH/CCLM4-8-17 show only minor negative trends. The negative gradients range from -2.5 mm/decade (not significant) to -16.5 mm/decade at 2160 m a.s.l., corresponding to -1.3 to -6.2%/decade respectively. At 660 m a.s.l. the gradients of the long-term trends are generally lower with -2.2 to -5.8 mm/decade, but the relative decrease of -4.5 to -9.9%/decade is more pronounced than at high elevation. Besides the results based on NorESM1-M/DMI-HIRHAM5suggesting an increase of SR_{max} in JJA at high elevation, negative trends have been obtained based on the other four GCMs/RCMs. Relative changes are higher at low elevations, whereas the changes in terms of absolute amounts are higher in the upper elevation range.

For the fall season, the results based on NorESM1-M/DMI-HIRHAM5 do not suggest any significant changes of SR_{max}. The results based on the other models show a significant reduction of SR_{max} with steeper gradients at a higher elevation. At 660 m a.s.l. the gradients of the long-term trends range from -3.5 to -5.8 mm/decade. At 2160 m a.s.l., the gradients are steeper with -5.6 to -14.7 mm/decade projected change of SR_{max}. However, the relative changes are higher at low elevation (-8.2 to -10.8%/decade comparing the means of SR_{max} in SON during the REF and END periods) compared to the uppermost elevation step considered (-3.1 to -7.7%/decade).

4.5 Projected changes in the seasonal frequency of subsurface runoff exceeding 100 mm

According to the findings presented in Sect. 4.2, the landslide moves fastest during periods with SR_{cum} exceeding 100 mm. Figure 9 shows the seasonal relative frequency of SR_{cum} exceeding 100 mm for the REF period and the deviations from that for the MID and END period. In the winter season, the results suggest only a few occurrences of SR_{cum} exceeding 100 mm ($f \leq 10\%$) in the REF period, evenly distributed across the elevation steps. In the MID period, the frequency of $SR_{cum} > 100$ mm increases slightly. At low elevation, the increase is more distinct considering the GCMs/RCMs EC-EARTH/RACMO22E and NorESM1-M/DMI-HIRHAM5. The results based on the latter indicate a markedly increasing frequency of $SR_{cum} > 100$ mm towards the end of the century, while the results based on the other four GCMs/RCMs point to a slight decrease at low and an increase at high elevations.

In the spring season, during the REF period, the frequency of $SR_{cum} > 100$ mm is clearly higher than during winter, with an emphasis on the medium elevations. In the MID period, the results generally suggest a slight increase in the frequency of $SR_{cum} > 100$ mm in high
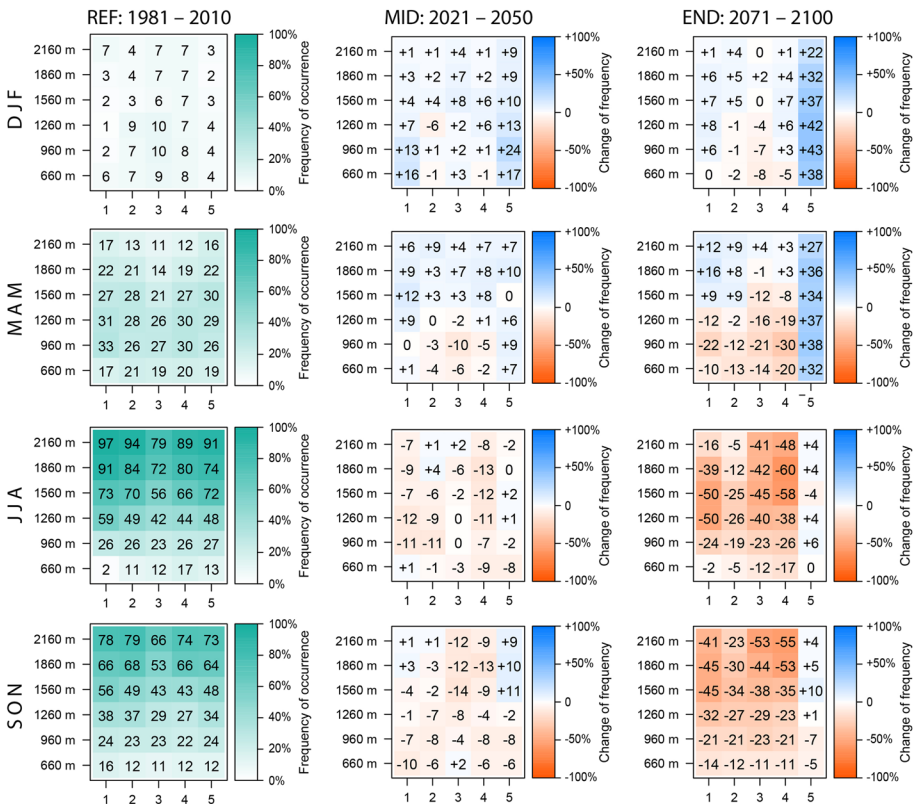

Fig. 9 Seasonal frequency of subsurface runoff surpassing the identified threshold of 100 mm per GCM/RCM and elevation step during the reference period (REF; left panels) and respective changes projected for the periods 2021–2050 (MID) and 2071–2100 (END). The numbers on the x-axis refer to the considered GCMs/RCMs, see Table 3

elevations and no change or a slight decrease at low elevations, with the exception of the results based on NorESM1-M/DMI-HIRHAM5 also suggesting a slight positive change at low elevations. The general pattern for spring is more pronounced in the END period, except for the results from NorESM1-M/DMI-HIRHAM5, indicating a distinctly higher frequency of $SR_{cum} > 100$ mm.

In the summer season, the frequency of $SR_{cum} > 100$ mm is reaching almost 100% in the uppermost elevation step and decreases to 2–17% in the lowest elevation step during the REF period. During the MID period, the frequency of $SR_{cum} > 100$ mm is generally projected to decrease, with some results indicating no or slightly positive change. The changes are clearly more distinct in the END period, with a reduction of up to −60% of $SR_{cum} > 100$ mm. The negative changes are projected mainly in the medium and upper elevation steps. Only the results based on NorESM1-M/DMI/HIRHAM5 do not indicate major changes.

In the fall season, the frequency of $SR_{cum} > 100$ mm is considerably high, particularly in the uppermost elevations. In the MID period, consistently negative changes in the frequency of $SR_{cum} > 100$ mm can only be found for the elevation steps 960 and 1260. Above, distinct positive changes are projected based on the GCM/RCM NorESM1-M/DMI-HIRHAM5. Also based on the GCMs/RCMs EC-EARTH/RACMO22E and EC-EARTH/CCLM4-8-17 slightly positive changes are projected in the upper elevation steps. Similar to the summer season, a distinct reduction of the frequency of $SR_{cum} > 100$ mm is projected in the END period, mainly in the upper elevations. The results based on NorESM1-M/DMI-HIRHAM5 suggest minor negative changes in low and minor positive changes in high elevations.

4.6 Results based on revised land cover parameterization

The analysis of the frequency of $SR_{cum} > 100$ mm per GCM/RCM and elevation step within the defined 30-years periods was repeated with the model results considering the adapted land cover parameterization. Figure 10 shows the respective changes of the frequency of occurrence compared to the results with the concurrent land cover parameterization. In general, the frequency of $SR_{cum} > 100$ mm reduces when considering mixed forests instead of the currently present coniferous forests.

The greatest impacts (in terms of the reduction of the frequency of $SR_{cum} > 100$ mm) are indicated at medium elevations in JJA and SON for the REF and MID periods. For the END period the results based on the selected GCMs/RCMs diverge, with four GCMs/RCMs indicating main changes in the upper elevation range and one GCM/RCM suggesting the main reduction at low (DJF, MAM, JJA) and medium elevations (SON). Potential impacts due to the adjusted land cover during the REF period suggest minor changes in the winter season, particularly in high elevations. For the MID and END periods only minor changes are projected in DJF, except for the results based on NorESM1-M/DMI-HIRHAM5, suggesting a reduced frequency of $SR_{cum} > 100$ mm of up to −15% in low elevations in the END period. In the spring season, the frequency of $SR_{cum} > 100$ mm is slightly lower than in DJF, particularly in low and medium elevations. The resulting reductions in the END period show a slightly higher variability compared to the REF and MID period. In the summer season the frequency of $SR_{cum} > 100$ mm reduces mainly in the medium elevation range in the REF and MID periods. In the END period four out of five GCMs/RCMs suggest a reduction in the uppermost elevation, while the results based on one GCM/RCM (NorESM1-M/DMI-HIRHAM5) show a reduction in low and medium elevation ranges. In
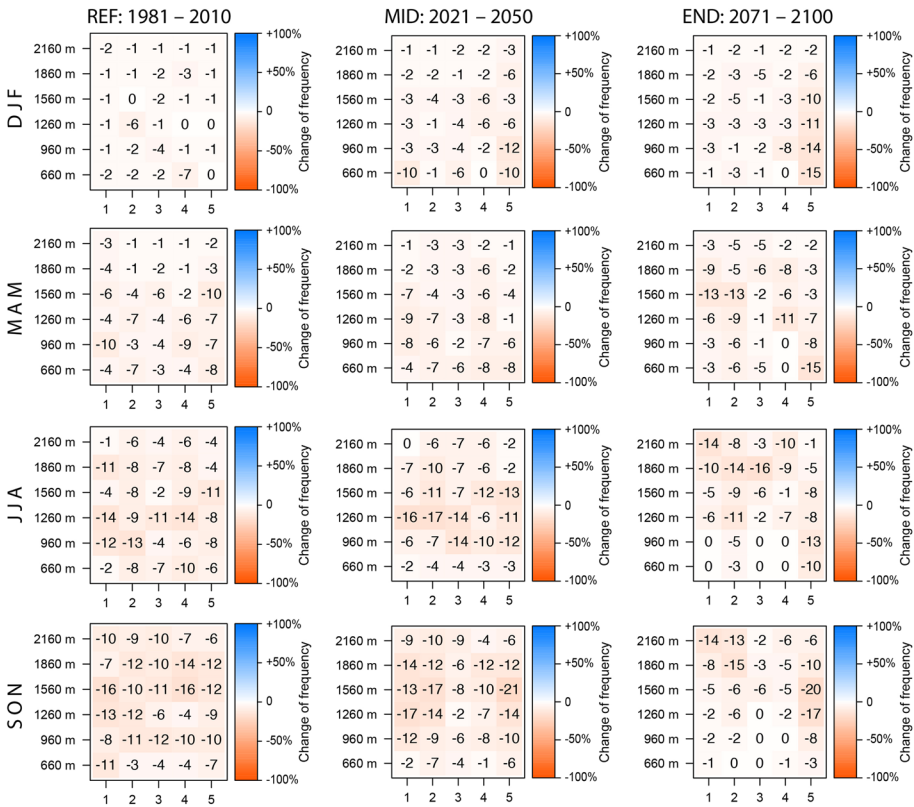
REF: 1981 – 2010

DJF

1981–2010	1	2	3	4	5
2160 m	-2	-1	-1	-1	-1
1860 m	-1	-1	-2	-3	-1
1560 m	-1	0	-2	-1	-1
1260 m	-1	-6	-1	0	0
960 m	-1	-2	-4	-1	-1
660 m	-2	-2	-2	-7	0

MID: 2021 – 2050

	1	2	3	4	5
2160 m	-1	-1	-2	-2	-3
1860 m	-2	-2	-1	-2	-6
1560 m	-3	-4	-3	-6	-3
1260 m	-3	-1	-4	-6	-6
960 m	-3	-3	-4	-2	-12
660 m	-10	-1	-6	0	-10

END: 2071 – 2100

	1	2	3	4	5
2160 m	-1	-2	-1	-2	-2
1860 m	-2	-3	-5	-2	-6
1560 m	-2	-5	-1	-3	-10
1260 m	-3	-3	-3	-3	-11
960 m	-3	-1	-2	-8	-14
660 m	-1	-3	-1	0	-15

MAM

REF	1	2	3	4	5
2160 m	-3	-1	-1	-1	-2
1860 m	-4	-1	-2	-1	-3
1560 m	-6	-4	-6	-2	-10
1260 m	-4	-7	-4	-6	-7
960 m	-10	-3	-4	-9	-7
660 m	-4	-7	-3	-4	-8

MID	1	2	3	4	5
2160 m	-1	-3	-3	-2	-1
1860 m	-2	-3	-3	-6	-2
1560 m	-7	-4	-3	-6	-4
1260 m	-9	-7	-3	-8	-1
960 m	-8	-6	-2	-7	-6
660 m	-4	-7	-6	-8	-8

END	1	2	3	4	5
2160 m	-3	-5	-5	-2	-2
1860 m	-9	-5	-6	-8	-3
1560 m	-13	-13	-2	-6	-3
1260 m	-6	-9	-1	-11	-7
960 m	-3	-6	-1	0	-8
660 m	-3	-6	-5	0	-15

JJA

REF	1	2	3	4	5
2160 m	-1	-6	-4	-6	-4
1860 m	-11	-8	-7	-8	-4
1560 m	-4	-8	-2	-9	-11
1260 m	-14	-9	-11	-14	-8
960 m	-12	-13	-4	-6	-8
660 m	-2	-8	-7	-10	-6

MID	1	2	3	4	5
2160 m	0	-6	-7	-6	-2
1860 m	-7	-10	-7	-6	-2
1560 m	-6	-11	-7	-12	-13
1260 m	-16	-17	-14	-6	-11
960 m	-6	-7	-14	-10	-12
660 m	-2	-4	-4	-3	-3

END	1	2	3	4	5
2160 m	-14	-8	-3	-10	-1
1860 m	-10	-14	-16	-9	-5
1560 m	-5	-9	-6	-1	-8
1260 m	-6	-11	-2	-7	-8
960 m	0	-5	0	0	-13
660 m	0	-3	0	0	-10

SON

REF	1	2	3	4	5
2160 m	-10	-9	-10	-7	-6
1860 m	-7	-12	-10	-14	-12
1560 m	-16	-10	-11	-16	-12
1260 m	-13	-12	-6	-4	-9
960 m	-8	-11	-12	-10	-10
660 m	-11	-3	-4	-4	-7

MID	1	2	3	4	5
2160 m	-9	-10	-9	-4	-6
1860 m	-14	-12	-6	-12	-12
1560 m	-13	-17	-8	-10	-21
1260 m	-17	-14	-2	-7	-14
960 m	-12	-9	-6	-8	-10
660 m	-2	-7	-4	-1	-6

END	1	2	3	4	5
2160 m	-14	-13	-2	-6	-6
1860 m	-8	-15	-3	-5	-10
1560 m	-5	-6	-6	-5	-20
1260 m	-2	-6	0	-2	-17
960 m	-2	-2	0	0	-8
660 m	-1	0	0	-1	-3

Legend scale (each panel): +100% / +50% / 0 / -50% / -100% — Change of frequency

Fig. 10 Changes of the seasonal frequency of subsurface runoff surpassing the identified threshold of 100 mm per GCM/RCM and elevation step considering a land cover scenario compared to the results considering the concurrent land cover during the reference period (REF; left panels) and the periods 2021–2050 (MID) and 2071–2100 (END). The numbers on the x-axis refer to the considered GCMs/RCMs, see Table 3

the fall season, the main reduction of the frequency of $SR_{cum} > 100$ mm due to the changed land cover parameterization is suggested in medium and upper elevation ranges in the REF and MID periods. In the END period, the results based on four GCMs/RCMs indicate the main reduction in the upper elevation steps while one GCM/RCM shows the major reduction in medium elevation range.

5 Discussion

The results of the monthly water balance model based on four out of five selected GCMs/RCMs suggest that the amounts of subsurface runoff, identified as the main hydro-meteorological driver of the landslide, will generally decrease under projected future climate conditions considering RCP8.5. This finding is generally in line with results presented in the review by Gariano and Guzzetti (2016), implying a reduced activity of deep-seated landslides in the European Alps and the Apennin under future climate conditions as found in dedicated case studies (e.g. Comegna et al. 2013; Malet et al. 2005). However, the results

based on the projections of one GCM/RCM indicate no change during the summer and fall seasons and a distinct increase in subsurface runoff in the winter and spring season, which may generally enhance the landslide's activity. This proves that the results of studies based on a single GCM/RCM simulation or on an ensemble mean cannot not represent the range and uncertainties of the spectrum of available GCMs/RCMs. Multiple climate simulations should be considered for evaluating climate change impacts on the water balance. Below, the results presented in this study are further discussed considering potentialities and limitations regarding (i) the model, (ii) the used data and (iii), characteristics of the study area.

5.1 Potentialities and limitations of the model

The newly introduced modules and parameters allow to consider soil and land cover characteristics, which proved to be sensitive, having a high impact on the model results. The crop coefficient modifies the potential and actual evapotranspiration, which is the main effect of vegetation on the water balance. For investigating the impacts of forests as nature-based solution against landslide activity under future climate conditions, this additional model element is inevitable. The SCS curve number and related parameters affect the amount of surface runoff, which is governed by the duration and intensity of precipitation and soil characteristics (e.g. Meißl et al. 2020). The introduced model parameter for setting the soil water content at field capacity did not lead to changes of the subsurface runoff in the sensitivity analysis, considering current climatic conditions. This is due to the fact that under current conditions periods of moisture deficits are rare in the study area. However, under drier future conditions the soil water content at field capacity could become a sensitive parameter and should be parameterized carefully.

The monthly water balance model generally proved feasible for reproducing the hydro-meteorological forcing of the Vögelsberg landslide under present day conditions. The subsurface runoff component shows similar non-seasonal cycles comparable to the acceleration and deceleration phases of the landslide. However, a monthly temporal scale is considered coarse for reproducing the landslide's activity and the hydro-meteorological drivers behind, explaining the comparably low coefficient of determination of 0.66. In a recent study, Pfeiffer et al. (2021) analysed the hydro-meteorological drivers of the Vögelsberg landslide based on daily time series of water balance components, resulting in markedly higher correlations with landslide velocity. However, the monthly water balance model employed in this study cannot resolve sub-monthly dynamics, resulting in lower correlation coefficients. Nevertheless, applying the water balance model with climate simulations of air temperature and precipitation will yield more reliable results on a monthly scale. The temporal scale must therefore be considered as a compromise between the response time of the landslide and the temporal domain of the adopted model and data.

No significant changes in direct runoff could be observed in the model results until the end of the century, indicating that the infiltration capacity of the soils is not surpassed under future climate conditions. However, convective rainfall events characterized by sub-daily durations which typically lead to an increase in direct runoff are not properly covered by the selected GCMs/RCMs. Furthermore, the monthly time scale of the presented model is not able to identify the role of convective rainfalls related to the temporal dynamics of the landslide. However, the findings of a recent study by Pfeiffer et al. (2021) show that short-term extreme events apparently do not lead to direct reactions of the landslide. This is underlined by the delayed acceleration as a response to the hydro-meteorological forcing of up to 60 days. However, future studies based on model chains implemented at finer

spatial and temporal scales will provide further insights regarding the role of convective rainfall events towards landslide activity.

5.2 Potentialities and limitations with respect to the selected GCM/RCM simulations

The bias-corrected EURO-CORDEX data for the RCP8.5 scenario suggest that the mean air temperature will increase in the study area in all seasons, particularly towards the end of the century (2071–2100). Since positive trends are found by all selected GCMs/RCMs, this result is considered robust under RCP8.5. Inferred trends of the amount of precipitation are not as well in agreement, with three out of five GCMs/RCMs suggesting an increase in DJF and MAM and a decrease in JJA. One out of five GCMs/RCMs suggests an increase in precipitation in SON. The variance of seasonal precipitation amounts is high (particularly in JJA) and some of the trends are therefore not statistically significant (particularly in SON). As a result of this disagreement, the trends of the projected subsurface runoff are not in full agreement. Four out of five GCMs/RCMs suggest a generally lower monthly subsurface runoff under future climate conditions, mainly because of increasing evapotranspiration due to rising air temperature and no substantial changes in precipitation. On the contrary, the increase in precipitation projected by the GCM/RCM NorESM1-M/ DMI-HIRHAM5 can compensate the increase in evapotranspiration (caused by rising air temperature) in summer and fall. For the winter and spring season however, the projected increase in precipitation is converted into subsurface flow using this particular GCM/RCM. The computed water balance is therefore highly sensitive to the selection of climate simulations, which is line with other studies with hydrological foci (e.g. Her et al. 2019; Lee et al. 2021).

The introduction of a different land cover in the model on the other hand, resulted in a slight but consistent reduction of the frequency of events with a high subsurface runoff. The frequency decreases particularly in the summer and fall seasons in the REF and MID periods and would thus contribute to a reduction of the landslide's activity. Related scenarios of ecological engineering qualifying as nature-based solutions were considered by Malet et al. (2005), including grass seeding, planting of trees and a mix of both. Particularly the planting of trees resulted in a distinct decrease in the groundwater level, which would lead to more stable conditions (Malet et al. 2005).

The reference period (1981–2010; 30 years) and the period for parameterizing the model (2016–2019; 3.5 years) are much shorter than the projection period (2021–2100; 80 years). Particularly the short period for parameterizing the model may introduce uncertainties in the long-term projections of the hydro-meteorological forcing and the related conclusions about future landslide activity. Related studies were affected by the same issue (e.g. Malet et al. 2005; Comegna et al. 2013), and longer monitoring time series for this type of landslide are still scarce.

The climate simulation chains, as well as the representative concentration pathway were selected in order to fulfil the overall objectives of the OPERANDUM project. In the presented Austrian case study, the applied bias-correction minimized the differences between simulations and observations in the control period. However, further suitable GCM/RCM simulations could have been identified in an individual pre-screening step. This could also provide a deeper understanding about the actual performance of the different simulations, permitting a more confident analysis about the future trends projected by them.

5.3 Potentialities and limitations regarding the characteristics of the study area

In the present study, particular attention was paid to the elevation range of the landslide catchment area. The results clearly show that the water balance depends on elevation. Previous studies proved that the landslide reacts to hydro-meteorological input from all elevation ranges, but showed almost immediate reactions after snow melt at low elevation (Pfeiffer et al. 2021, 2022). This could indicate that the landslide reacts more sensitive to groundwater recharge at close-by upslope contributing areas (e.g. up to 1300 m a.s.l.). The presented results based on four out of five GCMs/RCMs under RCP8.5 show a distinct relative reduction of SR_{max} at low elevation, while the absolute reduction is more pronounced at high elevations. Furthermore, the frequency of SR_{cum} surpassing 100 mm decreases particularly towards the end of the century mainly below 1300 m a.s.l. in MAM (−16% mean change), at mid and upper elevations in JJA (−36% mean change) and across the elevation range in SON (−30% mean change). These results indicate a distinct reduction of subsurface runoff across the vertical range of the landslide catchment area. This would lead to a reduced velocity and less frequent acceleration phases in MAM, JJA and SON under future conditions. On the other hand, the amount of SR_{max} and the frequency of SR_{cum} surpassing 100 mm increases slightly in DJF (+2% mean change) and in MAM at high elevation (+7% mean change). Particularly in future warmer winter seasons, the landslide could accelerate more frequently. However, the results based on one GCM/RCM contradict these conclusions and instead suggest an increase of SR_{max} and the frequency of SR_{cum} surpassing 100 mm in DJF (+36% mean change) and MAM (+34% mean change) across the elevation range, while indicating no change in JJA and SON. These contradictions have to be considered at least as uncertainty of the model results. Further uncertainties may be related to potential feedback loops in the water balance (e.g. due to land cover change) and related changes of the hydrological system, as well as the heterogeneity of the landslide catchment area in terms of hypsometry, aspect and lithology which could not be considered in the empirical model. Spatially distributed hydro-meteorological models (e.g. Malet et al. 2005) could provide more detailed insights, but require extensive field and laboratory tests for their parameterization and may introduce additional sources of uncertainty.

For interpreting the results in terms of the landslide's future activity, its mechanic principles are assumed to be invariant over time. It is assumed that the correlation between velocity and subsurface runoff component as well as the selected threshold will remain constant over time and that the landslide will not generally accelerate or decelerate despite changes of the hydro-meteorological forcing. However, the landslide's geometry will change continuously, particularly at the foot slope. Due to these changes also the hydrological system and the material properties could change. This could modify the landslide's behaviour and sensitivity with regard to the hydro-meteorological forcing, particularly if longer time spans are considered.

6 Conclusions

An extended monthly water balance model was employed for reproducing the current hydro-meteorological forcing of a continuously moving deep-seated earth slide in Tyrol (Austria). The model relies on time series of air temperature and precipitation and can consider effects of land cover and soil properties. Water balance components were computed

across the vertical range of the landslide's effective hydrological catchment area (660 to 2160 m a.s.l.) to take their elevation-dependent variability into account. The resulting subsurface runoff component cumulated over three months proved to be a suitable proxy for the temporal variation of landslide velocity, considering the period from May 2016 to October 2019. Then, projections of the water balance components were computed based on five selected, bias-corrected climate simulations (EURO-CORDEX) of air temperature and precipitation, considering the 'most severe' scenario in terms of future evolution of greenhouse gas concentration (RCP8.5). The resulting subsurface runoff components were analysed, considering trends of its seasonal maximum and the seasonal frequency of the 3 months-cumulated subsurface runoff exceeding a threshold of 100 mm. Based on the results, the following conclusions are drawn.

The bias-corrected projections of mean seasonal air temperature show a positive trend, with a distinct increase in the END period (2071–2100). Resulting trends based on three out of five selected GCMs/RCMs are in good agreement with observed trends in mean seasonal air temperature for the winter, spring and summer season considering the period of 1981–2019. The bias-corrected projections of the seasonal precipitation sum do not show clear trends and the results of the selected GCMs/RCMs are not in agreement. However, as a consequence, the results of the employed water balance model suggest generally dryer conditions in the study area, mainly due to enhanced evapotranspiration owing to rising air temperatures (according to the results based on four out of five selected GCMs/RCMs). This projected change in the water balance entails a general reduction in subsurface runoff, reducing the landslide's hydro-meteorological forcing under future climate conditions. Particularly during the summer and fall seasons a respective reduction of subsurface runoff is suggested across the catchment's elevation range. At low elevation, the results show a reduction of subsurface runoff in all seasons. Furthermore, an alternative land cover could further reduce subsurface runoff, but may show main effects under climate conditions during the REF and MID periods and mainly in JJA and SON. Altogether, this could lead to a reduction of the landslide's activity (e.g. reduced velocity and less frequent acceleration phases).

However, the results based on one GCM/RCM (NorESM1-M/DMI-HIRHAM5) contradict these results to some degree, suggesting an increase in subsurface runoff especially in the winter and spring seasons. Therefore, also an increase in the landslide's activity, particularly in DJF and MAM cannot be excluded. For this reason, it is considered vital to select a variety of different GCM/RCM simulations for studies investigating the impacts of projected climate change on the water balance and related consequences regarding the activity of deep-seated landslides.

The response of individual deep-seated landslides to climate change highly depends on respective local characteristics affecting the water balance, including topography (elevation range, hypsometry, and aspect), the geological setting (structural and stratigraphic properties), land cover as well as local climate peculiarities in mountain environments. Further research is required to include these landslide-specific characteristics in the assessment of projected climate change impacts on landslide activity and to upscale the analyses to a regional or even continental scale. Furthermore, given the complexity of the investigated geomorphological context, major improvements could be expected by adopting the next generation of climate simulation chains at very high resolution (1–4 km) permitting an explicit resolution of convective processes.

Declarations

References

Allen RG, Pereira LS, Raes D, Smith M (1998) Crop evapotranspiration–guidelines for computing crop water requirements. Irrigation and drainage paper 56, FAO, Rome 300(9), D05109.

Alvioli M, Melillo M, Guzzetti F, Rossi M, Palazzi E, von Hardenberg J, Brunetti MT, Peruccacci S (2018) Implications of climate change on landslide hazard in central Italy. Sci Total Environ 630:1528–1543. https://doi.org/10.1016/j.scitotenv.2018.02.315

Andre K, Koch R, Olefs M (2019) Analyse von Schneemessreihen des HD Tirol–vergangenheit. Central Institute for meteorology and geodynamics, Vienna. URL: https://www.tirol.gv.at/umwelt/wasserwirtschaft/wasserkreislauf/fuse-hd-tirol (last accessed: 2022/08/01)

Bock AR, Hay LE, McCabe GJ, Markstrom SL, Atkinson RD (2016) Parameter regionalization of a monthly water balance model for the conterminous United States. Hydrol Earth Syst Sci 20(7):2861–2876. https://doi.org/10.5194/hess-20-2861-2016

Borgatti L, Soldati M (2010) Landslides as a geomorphological proxy for climate change: a record from the Dolomites (northern Italy). Geomorphology 120(1):56–64. https://doi.org/10.1016/j.geomorph.2009.09.015

Buma J, Dehn M (1998) A method for predicting the impact of climate change on slope stability. Environ Geol 35(2):190–196. https://doi.org/10.1007/s002540050305

Ciabatta L, Camici S, Brocca L, Ponziani F, Stelluti M, Berni N, Moramarco T (2016) Assessing the impact of climate-change scenarios on landslide occurrence in Umbria Region Italy. J Hydrol 541:285–295. https://doi.org/10.1016/j.jhydrol.2016.02.007

Coe JA (2012) Regional moisture balance control of landslide motion: implications for landslide forecasting in a changing climate. Geology 40(4):323–326. https://doi.org/10.1130/G32897.1

Coe JA, Godt JW (2012) Review of approaches for assessing the impact of climate change on landslide hazards, in Eberhard E, Froese C, Turner K, Leroueil S (eds.) Landslides and engineered slopes, protecting society through improved understanding: Proceedings of the 11th international and 2nd north american symposium on landslides and engineered slopes, Banff, Canada, 3–8 June, USGS Publications Warehouse, Reston, VA, pp. 371–377.

Comegna L, Picarelli L, Bucchignani E, Mercogliano P (2013) Potential effects of incoming climate changes on the behaviour of slow active landslides in clay. Landslides 10(4):373–391. https://doi.org/10.1007/s10346-012-0339-3

Crozier MJ (2010) Deciphering the effect of climate change on landslide activity: a review. Geomorphology 124(3):260–267. https://doi.org/10.1016/j.geomorph.2010.04.009

Dehn M, Bürger G, Buma J, Gasparetto P (2000) Impact of climate change on slope stability using expanded downscaling. Eng Geol 55(3):193–204. https://doi.org/10.1016/S0013-7952(99)00123-4

EEA (2018) Corine Land Cover (CLC) 2018, Version 20b2, Technical report, European Environment Agency, https://land.copernicus.eu/pan-european/corine-land-cover/clc2018 (last accessed: 2021–07–02)

Ferguson BK (1996) Estimation of direct runoff in the thornthwaite water balance. Prof Geogr 48(3):263–271. https://doi.org/10.1111/j.0033-0124.1996.00263.x

Feyen L, Ciscar Martinez J, Gosling S, Ibarreta Ruiz D, Soria Ramirez A, Dosio A, Naumann G, Russo S, Formetta G, Forzieri G, Girardello M, Spinoni J, Mentaschi L, Bisselink B, Bernhard J, Gelati E, Adamovic M, Guenther S, De Roo A, Cammalleri C, Dottori F, Bianchi A, Alfieri L, Vousdoukas M, Mongelli I, Hinkel J, Ward P, Gomes Da Costa H, De Rigo D, Liberta G, Durrant T, San-Miguel-Ayanz J, Barredo Cano J, Mauri A, Caudullo G, Ceccherini G, Beck P, Cescatti A, Hristov J, Toreti A, Perez Dominguez I, Dentener F, Fellmann T, Elleby C, Ceglar A, Fumagalli D, Niemeyer S, Cerrani I, Panarello L, Bratu M, Després J, Szewczyk W, Matei N, Mulholland E, Olariaga-Guardiola M (2020) Climate change impacts and adaptation in Europe, EUR 30180 EN, JRC119178, Publications Office of the European Union, Luxembourg, https://doi.org/10.2760/171121

Gariano SL, Guzzetti F (2016) Landslides in a changing climate. Earth Sci Rev 162:227–252. https://doi.org/10.1016/j.earscirev.2016.08.011

Giorgi F, Jones C, Asrar GR (2009) Addressing climate information needs at the regional level: the CORDEX framework, WMO Bulletin 3(58).

Graves D, Chang H (2007) Hydrologic impacts of climate change in the upper clackamas river basin, Oregon, USA. Clim Res 33(2):143–158

Hamon WR (1961) Estimating potential evapotranspiration. J Hydraul Div 87(3):107–120. https://doi.org/10.1061/JYCEAJ.0000599

Hausfather Z, Peters GP (2020) Emissions–the 'business as usual' story is misleading. Nature 577:618–620. https://doi.org/10.1038/d41586-020-00177-3

Hay LE, McCabe GJ (2010) Hydrologic effects of climate change in the Yukon river basin. Clim Change 100(3):509–523. https://doi.org/10.1007/s10584-010-9805-x

Her Y, Yoo SH, Cho J, Hwang S, Jeong J, Seong C (2019) Uncertainty in hydrological analysis of climate change: multi-parameter vs. multi-GCM ensemble predictions. Sci Rep 9(1):4974. https://doi.org/10.1038/s41598-019-41334-7

Hock R, Rasul G, Adler C, Cáceres B, Gruber S, Hirabayashi Y, Jackson M, Kääb A, Kang S, Kutuzov S, Milner A, Molau U, Morin S, Orlove B, Steltzer H (2019) High Mountain Areas, In: Pörtner HO, Roberts DC, Masson-Delmotte V, Zhai P, Tignor M, Poloczanska E, Mintenbeck K, Alegría A, Nicolai M, Okem A, Petzold J, Rama B, Weyer NM (eds), IPCC Special Report on the Ocean and Cryosphere in a Changing Climate, 131–202.

IPCC (2014) Climate Change 2014: Synthesis report. Contribution of working groups I, II and III to the Fifth assessment report of the intergovernmental panel on climate change [Core Writing Team, R.K. Pachauri and L.A. Meyer (eds.)]. IPCC, Geneva, Switzerland, 151 pp.

IUSS Working Group WRB (2014) World reference base for soil resources 2014: international soil classification system for naming soils and creating legends for soil maps. In: Food and agriculture organization of the united nations (FAO), World Soil Resources Report. Rome, Italy, pp. 12–21.

Jaboyedoff M, Michoud C, Derron MH, Voumard J, Leibundgut G, Sudmeier-Rieux K, Nadim F, Leroi E (2016) Human-induced landslides: toward the analysis of anthropogenic changes of the slope

environment, in: Aversa S, Cascini L, Picarelli L, Scavia C (eds) Proceedings of the landslides and engineered slopes. Experience, theory and practice of the 12th international symposium on landslides; Jun 12–19; Napoli (Italy): CRC Press. p. 217–231.

Jacob D, Petersen J, Eggert B, Alias A, Christensen OB, Bouwer LM, Braun A, Colette A, Déqué M, Georgievski G, Georgopoulou E, Gobiet A, Menut L, Nikulin G, Haensler A, Hempelmann N, Jones C, Keuler K, Kovats S, Kröner N, Kotlarski S, Kriegsmann A, Martin E, van Meijgaard E, Moseley C, Pfeifer S, Preuschmann S, Radermacher C, Radtke K, Rechid D, Rounsevell M, Samuelsson P, Somot S, Soussana J-F, Teichmann C, Valentini R, Vautard R, Weber B, Yiou P (2014) EURO-CORDEX: new high-resolution climate change projections for European impact research. Reg Environ Change 14(2):563–578. https://doi.org/10.1007/s10113-013-0499-2

Jakob M (2022) Chapter 14 - Landslides in a changing climate. In: Davies T, Rosser N, Shroder JF (eds) Landslide hazards, risks, and disasters (Second Edition). Elsevier, pp 505–579

Jakob M, Owen T (2021) Projected effects of climate change on shallow landslides, North Shore Mountains, Vancouver, Canada. Geomorphology 393:107921. https://doi.org/10.1016/j.geomorph.2021.107921

Jennings KS, Winchell TS, Livneh B, Molotch NP (2018) Spatial variation of the rain-snow temperature threshold across the Northern Hemisphere. Nat Commun 9(1):1148. https://doi.org/10.1038/s41467-018-03629-7

Kendon EJ, Prein AF, Senior CA, Stirling A (2021) Challenges and outlook for convection-permitting climate modelling. Philos Trans Royal Soc a: Math, Phys Eng Sci 379(2195):20190547. https://doi.org/10.1098/rsta.2019.0547Lacroix

Lacroix P, Handwerger AL, Bièvre G (2020) Life and death of slow-moving landslides. Nature Rev Earth Environ 1(8):404–419. https://doi.org/10.1038/s43017-020-0072-8

Lateltin O, Beer C, Raetzo H, Caron C (1997) Landslides in Flysch terranes of Switzerland: causal factors and climate change. Eclogae Geologicae Helveticae 90:401–406

Lee S, Qi J, McCarty GW, Yeo IY, Zhang X, Moglen GE, Du L (2021) Uncertainty assessment of multi-parameter, multi-GCM, and multi-RCP simulations for streamflow and non-floodplain wetland (NFW) water storage. J Hydrol 600:126564. https://doi.org/10.1016/j.jhydrol.2021.126564

Malet J-P, van Asch TWJ, van Beek R, Maquaire O (2005) Forecasting the behaviour of complex landslides with a spatially distributed hydrological model. Nat Hazard 5(1):71–85. https://doi.org/10.5194/nhess-5-71-2005

Maraun D, Widmann M (2018) Statistical downscaling and bias correction for climate research. Cambridge University Press

McCabe GJ, Markstrom SL (2007), A monthly water-balance model driven by a graphical user interface, Vol. 1088, US Geological Survey Reston, VA.

Meehl GA, Boer GJ, Covey C, Latif M, Stouffer RJ (2000) The coupled model intercomparison project (CMIP). Bull Am Meteorol Soc 81(2):313–318

Meehl GA, Senior CA, Eyring V, Flato G, Lamarque J-F, Stouffer RJ, Taylor KE, Schlund M (2020) Context for interpreting equilibrium climate sensitivity and transient climate response from the CMIP6 Earth system models. Sci Adv. https://doi.org/10.1126/sciadv.aba1981

Meißl G, Zieher T, Geitner C (2020) Runoff response to rainfall events considering initial soil moisture–analysis of 9-year records in a small Alpine catchment (Brixenbach valley, Tyrol, Austria). J Hydrol: Reg Stud 30:100711. https://doi.org/10.1016/j.ejrh.2020.100711

Mora C, Spirandelli D, Franklin EC, Lynham J, Kantar MB, Miles W, Smith CZ, Freel K, Moy J, Louis LV, Barba EW, Bettinger K, Frazier AG, Colburn IXJF, Hanasaki N, Hawkins E, Hirabayashi Y, Knorr W, Little CM, Emanuel K, Sheffield J, Patz JA, Hunter CL (2018) Broad threat to humanity from cumulative climate hazards intensified by greenhouse gas emissions. Nat Clim Chang 8(12):1062–1071. https://doi.org/10.1038/s41558-018-0315-6

Nakićenović N, Davidson O, Davis G, Grübler A, Kram T, Lebre La Rovere E, Metz B, Morita T, Pepper W, Pitcher H, Sankovski A, Shukla P, Swart R, Watson R, Dadi Z (eds) (2000) Special report on emissions scenarios: a special report of working group III of the intergovernmental panel on climate change. Cambridge University Press, Cambridge

OPERANDUM 2022: H2020 OPERANDUM project. URL: https://www.operandum-project.eu (last access: 25/02/2022)

Pánek T (2019) Landslides and quaternary climate changes–the state of the art. Earth Sci Rev 196:102871. https://doi.org/10.1016/j.earscirev.2019.05.015

Pfeiffer J, Zieher T, Schmieder J, Rutzinger M, Strasser U (2021) Spatio-temporal assessment of the hydrological drivers of an active deep-seated gravitational slope deformation: the Vögelsberg landslide in Tyrol (Austria). Earth Surf Proc Land. https://doi.org/10.1002/esp.5129

Pfeiffer J, Zieher T, Schmieder J, Bogaard T, Rutzinger M, Spötl C (2022) Spatial assessment of probable recharge areas – investigating the hydrogeological controls of an active deep-seated gravitational slope deformation. Nat Hazard 22(7):2219–2237. https://doi.org/10.5194/nhess-22-2219-2022

Pichelli E, Coppola E, Sobolowski S, Ban N, Giorgi F, Stocchi P, Alias A, Belušić D, Berthou S, Caillaud C, Cardoso RM, Chan S, Christensen OB, Dobler A, de Vries H, Goergen K, Kendon EJ, Keuler K, Lenderink G, Lorenz T, Mishra AN, Panitz HJ, Schär C, Soares PMM, Truhetz H, Vergara-Temprado J (2021) The first multi-model ensemble of regional climate simulations at kilometer-scale resolution part 2: historical and future simulations of precipitation. Clim Dyn 56(11):3581–3602

Prokešová R, Medveďová A, Tábořík P, Snopková Z (2013) Towards hydrological triggering mechanisms of large deep-seated landslides, Landslides 10(3), 239–254. https://doi.org/10.1007/s10346-012-0330-z

Riahi K, Rao S, Krey V, Cho C, Chirkov V, Fischer G, Kindermann G, Nakicenovic N, Rafaj P (2011) RCP 8.5–A scenario of comparatively high greenhouse gas emissions. Clim Change 109(1):33. https://doi.org/10.1007/s10584-011-0149-y

Rianna G, Reder A, Mercogliano P, Pagano L (2017) Evaluation of variations in frequency of landslide events affecting pyroclastic covers in campania region under the effect of climate changes. Hydrology. https://doi.org/10.3390/hydrology4030034

Rockenschaub M, Kolenprat B, Nowotny A (2003) Innsbrucker quarzphyllitkomplex, tarntaler mesozoikum, patscherkofelkristallin, Geologische Bundesanstalt - Arbeitstagung 2003: Blatt 148 Brenner, 41–58.

Roeckner E, Bengtsson L, Feichter J, Lelieveld J, Rodhe H (1999) Transient climate change simulations with a coupled atmosphere-ocean GCM including the tropospheric sulfur cycle. J Clim 12(10):3004–3032. https://doi.org/10.1175/1520-0442(1999)012%3c3004:TCCSWA%3e2.0.CO;2

Sanderson BM (2018) Uncertainty quantification in multi-model ensembles. Clim Sci, Oxford Univer Press. https://doi.org/10.1093/acrefore/9780190228620.013.707

Schwalm CR, Glendon S, Duffy PB (2020) RCP85 tracks cumulative CO2 emissions. Proc Natl Acad Sci 117(33):19656–19657. https://doi.org/10.1073/pnas.2007117117

Sidle RC, Bogaard TA (2016) Dynamic earth system and ecological controls of rainfall-initiated landslides. Earth Sci Rev 159:275–291. https://doi.org/10.1016/j.earscirev.2016.05.013

Stoffel M, Huggel C (2012) Effects of climate change on mass movements in mountain environments. Prog Phys Geogr 36(3):421–439. https://doi.org/10.1177/0309133312441010

Stoffel M, Mendlik T, Schneuwly-Bollschweiler M, Gobiet A (2014) Possible impacts of climate change on debris-flow activity in the Swiss Alps. Clim Change 122(1):141–155. https://doi.org/10.1007/s10584-013-0993-z

Switanek MB, Troch PA, Castro CL, Leuprecht A, Chang H-I, Mukherjee R, Demaria EMC (2017) Scaled distribution mapping: a bias correction method that preserves raw climate model projected changes. Hydrol Earth Syst Sci 21(6):2649–2666. https://doi.org/10.5194/hess-21-2649-2017

Terzaghi K (1950) Mechanism of landslides, application of geology to engineering practice. Geol Soc Am. https://doi.org/10.1130/Berkey.1950.83

Thornthwaite CW, Mather JR (1955) The water balance. Publications in climatology, Laboratory of Climatology, p 8

Turkington T, Remaître A, Ettema J, Hussin H, van Westen C (2016) Assessing debris flow activity in a changing climate. Clim Change 137(1):293–305. https://doi.org/10.1007/s10584-016-1657-6

USDA (1986), Urban hydrology for small watersheds, Engineering Division, Soil Conservation Service, United States Department of Agriculture (USDA).

Van Beek LH (2002) The impact of land use and climatic change on slope stability in the Alcoy region. Netherlands Geographical Studies, Utrecht, Spain

van Vuuren DP, Edmonds J, Kainuma M, Riahi K, Thomson A, Hibbard K, Hurtt GC, Kram T, Krey V, Lamarque JF, Masui T, Meinshausen M, Nakicenovic N, Smith SJ, Rose SK (2011) The representative concentration pathways: an overview. Clim Change 109(1):5. https://doi.org/10.1007/s10584-011-0148-z

WMO (2017) WMO guidelines on the calculation of climate normals, WMO-No. 1203. Geneva, Switzerland. URL: https://library.wmo.int/index.php?lvl=notice_display&id=20130 (last accessed: 05/04/2022)

Wyser K, van Noije T, Yang S, von Hardenberg J, O'Donnell D, Döscher R (2020) On the increased climate sensitivity in the EC-Earth model from CMIP5 to CMIP6. Geosci Model Dev 13(8):3465–3474. https://doi.org/10.5194/gmd-13-3465-2020

You J, Tarboton DG, Luce CH (2014) Modeling the snow surface temperature with a one-layer energy balance snowmelt model. Hydrol Earth Syst Sci 18(12):5061–5076. https://doi.org/10.5194/hess-18-5061-2014

ZAMG (2022) Winter 2018/19 mild und teils viel Niederschlag, teils sehr trocken. Central institute for meteorology and geodynamics. URL: https://www.zamg.ac.at/cms/de/klima/news/winter-2018-19-mild-und-teils-viel-niederschlag-teils-sehr-trocken (last accessed: 2022/08/01)

Zieher T, Rutzinger M, Schneider-Muntau B, Perzl F, Leidinger D, Formayer H, Geitner C (2017) Sensitivity analysis and calibration of a dynamic physically based slope stability model. Nat Hazards Earth Syst Sci 17(6):971–992. https://doi.org/10.5194/nhess-17-971-2017